AUT Journal of Civil Engineering

AUT J. Civil Eng., 1(2) (2017) 167-176
DOI: 10.22060/ceej.2017.12762.5262

Two Dimensional Stress and Displacement Wave Propagation Under Shock Loading in Saturated Porous Materials with Two Dimensional Functionally Graded Materails Using MLPG Method

H. Kazemi[1], F. Shahabian[1*], S. M. Hosseini[2]

[1] Civil Engineering Department, Faculty of Engineering, Ferdowsi University of Mashhad, Mashhad, Iran
[2] Industrial Engineering Department, Faculty of Engineering, Ferdowsi University of Mashhad,Mashhad, Iran

ABSTRACT: The meshless local Petrov-Galerkin (MLPG) method is employed for dynamic analysis of fully saturated porous materials under shock loading considering two directional functionally grading patterns in constitutive mechanical properties. To approximate the trial functions in the radial point interpolation method (RPIM), the radial basis functions (RBFs) are utilized. The mechanical properties are simulated using a non-linear grading model with the radial and axial exponent. The 2D propagation of displacement and stresses are tracked through radial and axial direction in a two dimensional domain for various grading patterns at different time instants. By employing the presented meshless technique, the effects of various grading patterns on maximum values of stresses and displacements are studied in detail. The variation in the value of radial exponent has a significant effect on the dynamic behavior of radial displacement and radial stress comparing to the variation in the value of axial exponent. The MLPG method has a high capability to track the stress and displacement wave fronts at every arbitrary time instant in 2D domain.

Review History:
Received: 12 April 2017
Revised: 5 September 2017
Accepted: 20 November 2017
Available Online: 1 December 2017

Keywords:
Porous materials
Stress wave propagation
Displacement wave propagation
MLPG method
Radial basis functions

1- Introduction

The earliest theory to consider the porosity of materials was developed by Terzaghi [1]. Based on the work of Terzaghi, a general theory of saturated anisotropic porous material was presented by Biot in 1941 [2]. In materials engineering, environmental geomechanics, biomechanics, soil structure interaction and geomechanics porous materials play an important role [3, 4]. Schanz and Cheng presented a transient wave propagation of a finite one-dimensional anisotropic poroelastic column with different types of boundary conditions [5]. A state of the art overview of the analytical solutions and numerical methods in the theory of poroelastodynamics may be found in Schanz's review paper [4].

The meshless method was well implied to many structural problems in recent decades. In this method, the scattered nodes with regular or irregular distributions are used to discrete the field functions in local sub-domains [6]. Because of using the nodes rather than the elements, the application of the meshless method in some problems for porous materials yields more accurate results.

A cylindrical borehole drilled in a porous material and stability of borehole is one of the major problems in many branches of engineering such as petroleum geology and wastewater treatment. The mechanical parameters of the excavation disturbed zone (EDZ) are normally reduced from its original value before excavation. This variation is modeled with the functionally graded material (FGMs). Kwon et al. and Lai et al. showed that the inflow in the EDZ is larger than that of the undisturbed zone [7, 8]. Poroelastic solution for borehole and cylinder with the linear variation of the shear modulus and permeability coefficient in the EDZ is presented by Kaewjuea [9]. Sladek et al. presented a dynamic behavior of FGMs using a meshless local Petrov-Galerkin (MLPG) method [10]. Moussavinezhad et al. developed the MLPG method for two dimensional dynamic stress analyses in 2D-FG cylinders [11]. Chen et al. applied the meshless local natural neighbor interpolation method to solve linear dynamic problems of FGMs in continuously heterogeneous and linear viscoelastic media [12]. The MLPG method was developed for axisymmetric problems in continuously non-homogeneous saturated porous media by Sladek et al. [13]. They also investigated the effect of materials with variable stiffness and permeability on displacements stresses and pore pressure in porous media in another paper [14]. The effects of uncertainty in mechanical properties on thermo-elastic wave propagation in FGMs were investigated by Hosseini and Shahabian [15, 16]. They also studied the stochastic dynamic response, the reliability analysis and safety evaluation of a functionally graded thick hollow cylinder, considering uncertain material properties subjected to shock loading [17, 18].

In this paper, an MLPG method with heaviside step function as the weight function is employed to investigate the effects of the material gradation on displacements and stresses wave propagation in the porous medium around the borehole. For

Corresponding author, E–mail: shahabf@um.ac.ir

this purpose, two dimensional exponential grading patterns for the shear modulus, coupling parameters between the solid and fluid and permeability are considered in the EDZ. To interpolate the fields' variables in terms of its nodal values, the radial point interpolation method (RPIM) with radial basis function (RBF) is used. The effects of various grading patterns on the dynamic behaviors of displacements and stresses are obtained and discussed in detail. The MLPG method showed that it is a very effective method with a high accuracy for stress and displacement propagation analysis of saturated porous materials with one and two directional grading patterns.

2- Local boundary integral equations

A saturated porous medium is a medium made up of a skeleton particle and fluid particle. As can be seen in Figure 1, the skeleton particle consists both of a solid part and occluded porosity [19].

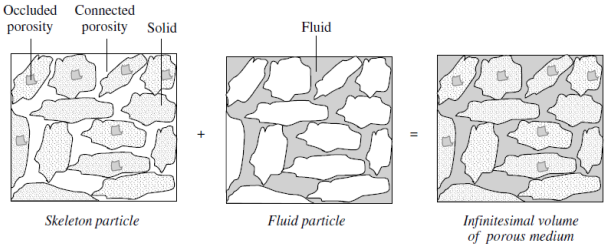

Fig. 1. The porous medium seen as the superposition of two continuous media [19]

The porosity φ is the ratio of the interconnected pores V^f to the total volume V. It is assumed that leading to $V = V^f + V^s$ with V^S the volume of the skeleton particle.

$$\varphi = \frac{V^f}{V} \tag{1}$$

In the present paper, the governing equation for porous materials is written based on the solid displacement u^s and the fluid displacement u^f. In the literature, this form is called u-u formulation [4].

For an axisymmetric problem in the cylindrical coordinate system, the axis of symmetry is identical with the z-axis. In this problem the non-zero strains are given as [13]:

$$\begin{aligned} &\varepsilon^s_{rr} = u^s_{r,r},\ \varepsilon^s_{\varphi\varphi} = u^s_r / r,\ \varepsilon^s_{rz} = (u^s_{r,z} + u^s_{z,r})/2 \\ &\varepsilon^s_{zz} = u^s_{z,z},\ \varepsilon^f_{kk} = u^f_{r,r} + u^f_{z,z} + u^f_r / r \\ &\varepsilon^f_{rr} = u^f_{r,r},\ \varepsilon^f_{\varphi\varphi} = u^f_r / r,\ \varepsilon^f_{zz} = u^f_{z,z} \end{aligned} \tag{2}$$

A comma after a quantity is used for partial derivations of the quantity and the dot shows the partial derivatives of variables with respect to the time. The stresses in the cylindrical coordinate system are given as [13]:

$$\sigma_{ij} = \sigma^s_{ij} + \delta_{ij}\sigma^f \tag{3}$$

$$\begin{pmatrix} \sigma^s_{rr} \\ \sigma^s_{\varphi\varphi} \\ \sigma^s_{zz} \\ \sigma^s_{rz} \end{pmatrix} = \begin{bmatrix} c_{11} & c_{12} & c_{13} & 0 \\ c_{12} & c_{11} & c_{13} & 0 \\ c_{13} & c_{13} & c_{11} & 0 \\ 0 & 0 & 0 & c_{44} \end{bmatrix} \begin{pmatrix} \varepsilon^s_{rr} \\ \varepsilon^s_{\varphi\varphi} \\ \varepsilon^s_{zz} \\ 2\varepsilon^s_{rz} \end{pmatrix} + \begin{bmatrix} Q \\ Q \\ Q \\ 0 \end{bmatrix} (\varepsilon^f_{kk}) \tag{4}$$

$$\sigma^f = \begin{bmatrix} Q \\ Q \\ Q \end{bmatrix}^T \begin{pmatrix} \varepsilon^s_{rr} \\ \varepsilon^s_{\varphi\varphi} \\ \varepsilon^s_{zz} \end{pmatrix} + \begin{bmatrix} R \\ R \\ R \end{bmatrix}^T \begin{pmatrix} \varepsilon^f_{rr} \\ \varepsilon^f_{\varphi\varphi} \\ \varepsilon^f_{zz} \end{pmatrix} \tag{5}$$

where

$$\begin{aligned} &c_{11} = \frac{4}{3}G + K + \frac{Q^2}{R}, c_{44} = G \\ &c_{12} = c_{13} = K - \frac{2}{3}G + \frac{Q^2}{R} \end{aligned} \tag{6}$$

where K denotes the bulk modulus, G is shear modulus; Q and R are coupling parameters between the solid and fluid and δ_{ij} is the Kronecker delta function.

The governing equations for porous media based on the balance of momentum for total stresses and for the fluid with vanishing body forces in the cylindrical coordinate system are given as [14]:

$$\begin{aligned} &\sigma_{rb,b}(r,z,\tau) + \frac{1}{r}[\sigma_{rr}(r,z,\tau) - \sigma_{\varphi\varphi}(r,z,\tau)] \\ &-(1-\varphi)\rho_s \ddot{u}^s_r(r,z,\tau) + \rho_f \varphi \ddot{u}^f_r(r,z,\tau) = 0 \end{aligned} \tag{7}$$

$$\begin{aligned} &\sigma_{zb,b}(r,z,\tau) + \frac{1}{r}\sigma_{rz}(r,z,\tau) \\ &-(1-\varphi)\rho_s \ddot{u}^s_r(r,z,\tau) + \rho_f \varphi \ddot{u}^f_r(r,z,\tau) = 0 \end{aligned} \tag{8}$$

$$\begin{aligned} &\sigma^f_b(r,z,\tau) - \varphi\rho_f \ddot{u}^f_b(r,z,\tau) \\ &-\rho_A[\ddot{u}^f_b(r,z,\tau) - \ddot{u}^s_b(r,z,\tau)] \\ &-\frac{\varphi^2}{\kappa}[\dot{u}^f_b(r,z,\tau) - \dot{u}^s_b(r,z,\tau)] = 0 \end{aligned} \tag{9}$$

Assuming summation for repeated subscript $b \in \{r, z\}$. Where φ, ρ_s, ρ_f, κ, τ denote the porosity, solid mass densities, fluid mass densities, the permeability and time, respectively. The symbol ρ_A denotes the apparent mass density that describes the dynamic interaction between the fluid and the skeleton [4].

By using the weight function W_i in local subdomains Ω_Q, the local weak-form of Equations 7 to 9 can be obtained as follows.

$$\int_{\Omega_Q} \begin{pmatrix} \frac{1}{r}[\sigma_{rr}(r,z,\tau) - \sigma_{\varphi\varphi}(r,z,\tau)] \\ +\sigma_{rb,b}(r,z,\tau) \\ +\rho_f \varphi \ddot{u}^f_r(r,z,\tau) \\ -(1-\varphi)\rho_s \ddot{u}^s_r(r,z,\tau) \end{pmatrix} W_1 d\Omega_Q = 0 \tag{10}$$

$$\int_{\Omega_Q}\begin{pmatrix}\sigma_{zb,b}(r,z,\tau)+\frac{1}{r}\sigma_{rz}(r,z,\tau)\\-(1-\varphi)\rho_s\ddot{u}_r^s(r,z,\tau)\\+\rho_f\varphi\ddot{u}_r^f(r,z,\tau)\end{pmatrix}W_2 d\Omega_Q=0 \tag{11}$$

$$\int_{\Omega_Q}\begin{pmatrix}\sigma_b^f(r,z,\tau)-\varphi\rho_f\ddot{u}_b^f(r,z,\tau)\\-\rho_A[\ddot{u}_b^f(r,z,\tau)-\ddot{u}_b^s(r,z,\tau)]\\-\frac{\varphi^2}{\kappa}[\dot{u}_b^f(r,z,\tau)-\dot{u}_b^s(r,z,\tau)]\end{pmatrix}W_3 d\Omega_Q=0 \tag{12}$$

In axisymmetric problems, the 3D local subdomain can be converted to the 2D domain by using the Equation 13-16.

$$d\Omega_Q=2\pi r\, d\Omega q \tag{13}$$

$$\int_{\Omega_Q}\begin{pmatrix}\frac{1}{r}[\sigma_{rr}(r,z,\tau)-\sigma_{\varphi\varphi}(r,z,\tau)]\\+\sigma_{rb,b}(r,z,\tau)\\+\rho_f\varphi\ddot{u}_r^f(r,z,\tau)\\-(1-\varphi)\rho_s\ddot{u}_r^s(r,z,\tau)\end{pmatrix}rW_1 d\Omega_q=0 \tag{14}$$

$$\int_{\Omega_Q}\begin{pmatrix}\sigma_{zb,b}(r,z,\tau)+\frac{1}{r}\sigma_{rz}(r,z,\tau)\\-(1-\varphi)\rho_s\ddot{u}_r^s(r,z,\tau)\\+\rho_f\varphi\ddot{u}_r^f(r,z,\tau)\end{pmatrix}rW_2 d\Omega_q=0 \tag{15}$$

$$\int_{\Omega_Q}\begin{pmatrix}\sigma_b^f(r,z,\tau)-\varphi\rho_f\ddot{u}_b^f(r,z,\tau)\\-\rho_A[\ddot{u}_b^f(r,z,\tau)-\ddot{u}_b^s(r,z,\tau)]\\-\frac{\varphi^2}{\kappa}[\dot{u}_b^f(r,z,\tau)-\dot{u}_b^s(r,z,\tau)]\end{pmatrix}rW_3 d\Omega_q=0 \tag{16}$$

By applying the Gauss divergence theorem to the last equations, derivation of stresses will be converted to the derivation of weight function. Since the heaviside step function is used as the weight function in this paper, the derivation of weight functions vanishes in the following equations.

$$\begin{aligned}&\int_\Gamma r(\sigma_{rr}n_r+\sigma_{rz}n_z)d\Gamma+\int_{\Omega q}-\sigma_{\varphi\varphi}d\Omega_q\\&-\int_{\Omega_q}(1-\varphi)\rho_s\ddot{u}_r^s(r,z,\tau)rd\Omega_q\\&+\int_{\Omega q}\rho_f\varphi\ddot{u}_r^f(r,z,\tau)rd\Omega_q=0\end{aligned} \tag{17}$$

$$\begin{aligned}&\int_\Gamma r(\sigma_{zr}n_r+\sigma_{zz}n_z)d\Gamma\\&-\int_{\Omega_q}(1-\varphi)\rho_s\ddot{u}_r^s(r,z,\tau)d\Omega_q\\&+\int_{\Omega_q}\rho_f\varphi\ddot{u}_r^f(r,z,\tau)d\Omega_q=0\end{aligned} \tag{18}$$

$$\int_\Gamma r\sigma^f n_r d\Gamma-\int_{\Omega_q}\sigma^f d\Omega \tag{19}$$

$$\begin{aligned}&-\int_{\Omega_q}\varphi\rho_f\ddot{u}_r^f(r,z,\tau)rd\Omega_q\\&-\int_{\Omega_q}\rho_A[\ddot{u}_r^f(r,z,\tau)-\ddot{u}_r^s(r,z,\tau)]rd\Omega_q\\&-\int_{\Omega_q}\frac{\varphi^2}{\kappa}[\dot{u}_r^f(r,z,\tau)-\dot{u}_r^s(r,z,\tau)]rd\Omega_q=0\end{aligned}$$

$$\begin{aligned}&\int_\Gamma r\sigma^f n_z d\Gamma-\int_{\Omega_q}\varphi\rho_f\ddot{u}_r^f(r,z,\tau)rd\Omega_q\\&-\int_{\Omega_q}\rho_A[\ddot{u}_r^f(r,z,\tau)-\ddot{u}_r^s(r,z,\tau)]rd\Omega_q\\&-\int_{\Omega_q}\frac{\varphi^2}{\kappa}[\dot{u}_r^f(r,z,\tau)-\dot{u}_r^s(r,z,\tau)]rd\Omega_q=0\end{aligned} \tag{20}$$

where Γ_q is the boundary of the local subdomain Ω_q. This boundary generally can be composed of three parts Γ_{qi}, Γ_{qu}, Γ_{qt} (Figure 2). Γ_{qi} is the internal boundary which is located entirely in the problem domain. Γ_{qu} and Γ_{qt} are the boundaries which are located on the boundary of problem domain with essential and natural boundary conditions, respectively ($\Gamma_q=\Gamma_{qi}\cup\Gamma_{qu}\cup\Gamma_{qt}$). Thus, Equations 17 to 20 can be rewritten as follows:

$$\begin{aligned}&\int_{\Gamma_{qi}+\Gamma_{qu}}r(\sigma_{rr}n_r+\sigma_{rz}n_z)d\Gamma+\int_{\Omega q}-\sigma_{\varphi\varphi}d\Omega_q\\&-\int_{\Omega_q}(1-\varphi)\rho_s\ddot{u}_r^s(r,z,\tau)rd\Omega_q\\&+\int_{\Omega q}\rho_f\varphi\ddot{u}_r^f(r,z,\tau)rd\Omega_q\\&=-\int_{\Gamma_{qt}}r(\sigma_{rr}n_r+\sigma_{rz}n_z)d\Gamma\end{aligned} \tag{21}$$

$$\begin{aligned}&\int_{\Gamma_{qi}+\Gamma_{qu}}r(\sigma_{zr}n_r+\sigma_{zz}n_z)d\Gamma\\&-\int_{\Omega_q}(1-\varphi)\rho_s\ddot{u}_r^s(r,z,\tau)d\Omega_q\\&+\int_{\Omega_q}\rho_f\varphi\ddot{u}_r^f(r,z,\tau)d\Omega_q\\&=-\int_{\Gamma_{qt}}r(\sigma_{zr}n_r+\sigma_{zz}n_z)d\Gamma\end{aligned} \tag{22}$$

$$\begin{aligned}&\int_{\Gamma_{qi}+\Gamma_{qu}}r\sigma^f n_r d\Gamma-\int_{\Omega_q}\sigma^f d\Omega_q\\&-\int_{\Omega_q}\varphi\rho_f\ddot{u}_r^f(r,z,\tau)rd\Omega_q\\&-\int_{\Omega_q}\rho_A[\ddot{u}_r^f(r,z,\tau)-\ddot{u}_r^s(r,z,\tau)]rd\Omega_q\\&-\int_{\Omega_q}\frac{\varphi^2}{\kappa}[\dot{u}_r^f(r,z,\tau)-\dot{u}_r^s(r,z,\tau)]rd\Omega_q\\&=-\int_{\Gamma_{qt}}r\sigma^f n_r d\Gamma\end{aligned} \tag{23}$$

$$\int_{\Gamma_{qi}+\Gamma_{qu}}r\sigma^f n_z d\Gamma-\int_{\Omega_q}\varphi\rho_f\ddot{u}_r^f(r,z,\tau)rd\Omega_q \tag{24}$$

$$-\int_{\Omega_q} \rho_A [\ddot{u}_r^f(r,z,\tau) - \ddot{u}_r^s(r,z,\tau)] r d\Omega_q$$

$$-\int_{\Omega_q} \frac{\varphi^2}{\kappa} [\dot{u}_r^f(r,z,\tau) - \dot{u}_r^s(r,z,\tau)] r d\Omega_q$$

$$= -\int_{\Gamma_{qt}} r\sigma^f n_z d\Gamma$$

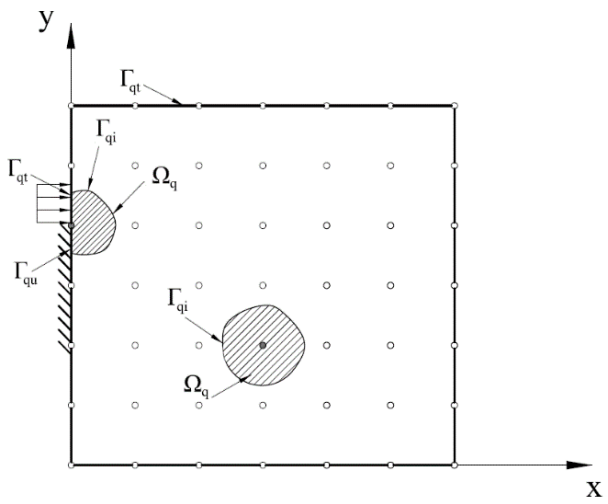

Fig. 2. The boundary of local subdomain in the MLPG method [6]

Equations 21 to 24 can be summarized in the following matrix form:

$$[M]\{\ddot{u}\} + [C]\{\dot{u}\} + [k]\{u\} = \{p\} \tag{25}$$

By using the stress-strain and strain-displacement, one can write the stresses with respect to the displacement. The mass and damping matrices are defined as:

$$[M] = \begin{bmatrix} -(1-\varphi)\rho_s & 0 & \rho_f\varphi & 0 \\ 0 & -(1-\varphi)\rho_s & 0 & \rho_f\varphi \\ \rho_A & 0 & -\rho_f\varphi - \rho_A & 0 \\ 0 & \rho_A & 0 & -\rho_f\varphi - \rho_A \end{bmatrix} \tag{26}$$

$$[C] = \begin{bmatrix} 0 & 0 & 0 & 0 \\ 0 & 0 & 0 & 0 \\ \frac{\varphi^2}{\kappa} & 0 & -\frac{\varphi^2}{\kappa} & 0 \\ 0 & \frac{\varphi^2}{\kappa} & 0 & -\frac{\varphi^2}{\kappa} \end{bmatrix} \tag{27}$$

The partial differential Equation 25 can be solved using the Newmark finite difference method in the time domain.

3- Discretization method

The radial point interpolation method (RPIM) is employed to construct the shape functions. In this method, an arbitrary function *u(x)* in local support domain of point x_Q can be approximated with respect to its nodal values located in support domain, using the radial basis function [*R(r)*]. To this end, the approximated function $u^h(x)$ can be written as follows.

$$u^h(x) = [R(r)]^T \{a(x_Q)\} \tag{28}$$

where, $\{a(x_Q)\}$ is the coefficient vector. There are some radial basis functions commonly used in the articles such as multiquadric, Gaussian, exponential and logarithmic [20]. In this paper, the radial basis function (RBF) is used in the following function.

$$R_i(r) = (r_i^2 + c^2)^q \tag{29}$$

where, c and q are the constant positive values which are experimentally determined to be 0.5 and 1.03, respectively [6]. r_i is the distance between the sampling point *x* and x_i.By applying Equation 28 to all nodes located in the support domain, the coefficient vector will be calculated.

$$\{u\} = [R_Q]\{a(x_Q)\} \tag{30}$$

where,

$$\{u\} = \{u_1\ u_2\ \dots\ u_n\}^T$$

$$[R_Q] = \begin{bmatrix} R_1(r_1) & R_2(r_1) & \cdots & R_n(r_1) \\ R_1(r_2) & R_2(r_2) & \cdots & R_n(r_2) \\ \vdots & \vdots & \ddots & \vdots \\ R_1(r_n) & R_2(r_n) & \cdots & R_n(r_n) \end{bmatrix} \tag{31}$$

in which *n* is the number of nodes located in the support domain. The coefficient vector $\{a(x_Q)\}$ can be derived from Equation 30.

$$\{a(x_Q)\} = [R_Q]^{-1}\{u\} \tag{32}$$

By inserting Equation 32 into Equation 28, the approximation function in terms of nodal value is further simplified to:

$$u^h(x) = \left([R(r)]^T [R_Q]^{-1}\right)\{u\} = [\phi]\{u\} \tag{33}$$

4- Verification

In the first example, a finite length cylinder with the fully-saturated porous material, which was used by Sladek et al. is considered to verify the presented method and results [14]. The radius of the cylinder and its height is considered one meter. The lateral sides and the bottom surface of the cylinder are impermeable and restrained in the normal direction. At the top surface, the stress with the following time variation is prescribed.

$$\sigma_{33}(t) = \begin{cases} P_0 \ for\ t \le 0.002\,\text{sec} \\ 0 \ for\ t > 0.002\,\text{sec} \end{cases} \tag{34}$$

where, $P_0 = -10^4$ Pa.

The degrees of freedom for this case are the displacement of solid and fluid which are denoted by u^s and u^f, respectively [14]. Due to symmetric conditions and using cylindrical coordinate, the problem is converted to the 1-d problem which can be analytically solved. The analytical solution for 1-d poroelastic column in the Laplace transform domain is presented by Schanz and Cheng [5]. In this problem, the domain is made of a special case of the porous material called Berea sandstone material. The poroelastic constants of such material are defined as [21]:

$$
\begin{aligned}
&k = 8.0\times10^{9}(N/m^2), G = 6.0\times10^{9}(N/m^2)\\
&R = 4.7\times10^{8}(N/m^2), \rho_s = 2800(kg/m^3)\\
&Q = 1.511\times10^{9}(N/m^2), \rho_f = 1000(kg/m^3)\\
&\kappa = 1.9\times10^{-10}(m^4/Ns),\ \alpha = 0.8,\ \varphi = 0.19
\end{aligned}
\tag{35}
$$

To verify the accuracy of the presented method, the time history of vertical displacement on the top surface is compared to the analytical results in Figure 3. A good agreement between the presented method and analytical result is achieved.

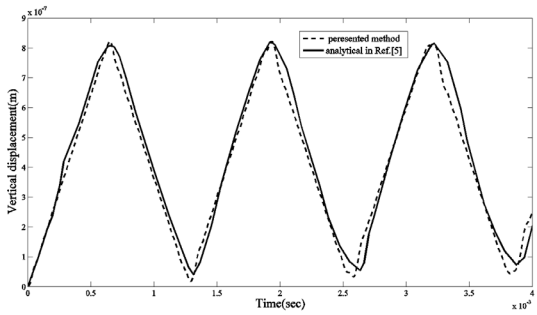

Fig. 3. The vertical displacement time history on the top surface for Berea sandstone compared to analytical results.

5- Results and discussion

In a real porous, the material properties are inhomogeneous. In the next example to investigate the effect of inhomogeneous on dynamic response, a cylindrical borehole drilled in a porous is considered in Figure 4. In this Figure, r_i is the inner radius, r_o is the outer radius and L is the length of the borehole which are considered to be 1, 2 and 1 meter, respectively.

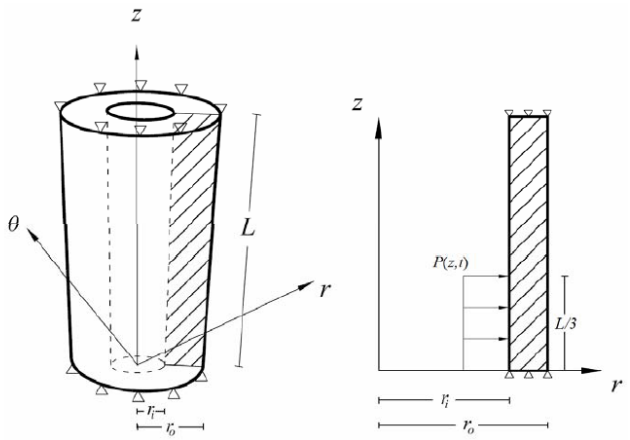

Fig. 4. A cylindrical borehole with the fully saturated porous material under shock loading.

The mechanical parameters of the excavation disturbed zone are normally reduced from its original value before excavation. One can model this variation with the functionally graded material (FGMs). For this purpose, two dimensional exponential grading patterns are considered in the excavation disturbed zone. In this paper the shear modulus, coupling parameters between the solid and fluid and permeability are varied functionally in radial and axial directions which are modeled by nonlinear exponential functions as follows:

$$
\begin{aligned}
G(r,z) = G_0[&\exp(-N_r(r_{out}-r))\\
&\times\exp(-N_z(z))]
\end{aligned}
\tag{36}
$$

$$
\begin{aligned}
\kappa(r,z) = \kappa_0[&\exp(N_r(r_{out}-r))\\
&\times\exp(N_z(z))]
\end{aligned}
\tag{37}
$$

$$
\begin{aligned}
Q(r,z) = Q_0[&\exp(-N_r(r_{out}-r))\\
&\times\exp(-N_z(z))]
\end{aligned}
\tag{38}
$$

where G_0, Q_0, κ_0 denote the original values before excavation which are considered to be the same in Equation 35. The parameters N_r and N_z are non-negative constants representing the gradation of disturbance due to the drilling process in radial and axial direction, respectively. By using these functions, the material properties of porous lead to the original values before excavation at large distance from the borehole. As can be seen in Figure 4, for this axisymmetric problem, it is sufficient to analyze only a symmetric part. Normal displacement of outer boundaries is restricted and impermeable boundary conditions are assumed on outer boundaries and borehole surface is drained. The assumed porous borehole cylinder is considered to be under shock radial loading on a third of the height at the inner radius, which can be defined as follows:

$$
p(z,t) = \begin{cases} P_0 t \ \textit{for}\ t \le 0.001\text{s and } z \le L/3 \\ 0 \ \textit{for}\ t > 0.001\text{s} \quad \textit{or} \quad z > L/3 \end{cases}
\tag{39}
$$

where, P_0= 1 GPa/s. Figure 5 shows time histories of radial displacement at node 1 (z = 0 m and r = 1 m in Figure 4) for various values N_r and N_z, in which both values are considered to be the same. The maximum values of radial displacement at same node for different values Nr and Nz are calculated and shown in Table 1. It is concluded when the axial and radial exponents are increased, the period of free vibration is increased up to 14% and the maximum values of radial displacement are increased up to 58%. The value of radial exponent (N_r) has more effect on the dynamic behavior of radial displacement comparing to the axial exponent (N_z). By considering the shock radial loading, this result seems reasonable. In Figure 6 the effect of radial exponent and axial exponent are compared at the same node. In this figure, the rate of increase in maximum radial displacement for different values of exponent than homogenous porous material is shown.

Table 1. The maximum of radial displacement at node 1 (z = 0 m and r = 1 m in Figure 4) in various factors of fgm

u_r(m)		N_r		
		0	**0.3**	**0.6**
N_z	0	3.788e-5	4.564e-5	5.432e-5
	0.3	4.061e-5	4.847e-5	5.735e-5
	0.6	4.315e-5	5.116e-5	6.017e-5

The 2D wave propagation of radial displacement at different time instants in 2D domain is shown in Figure 7. The wave fronts of radial displacement can be tracked for various values of 2D volume exponents. As can be seen in these figures, the grading pattern has a significant effect on wave propagation so that by increasing the value of the exponent, the wave propagation speed is decreased but the values of radial displacement contours are increased.

The maximum values of radial stress at the center of the

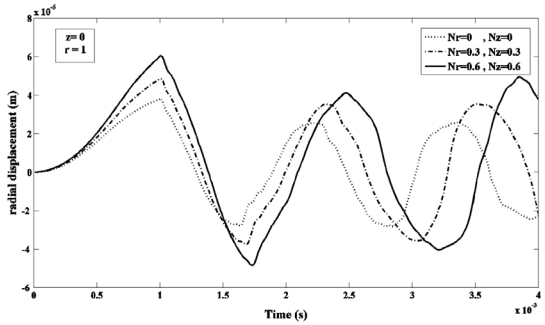

Fig. 5. The radial displacement time histories at node 1 (z = 0 m and r = 1 m in Figure 4) for various 2D-FGM

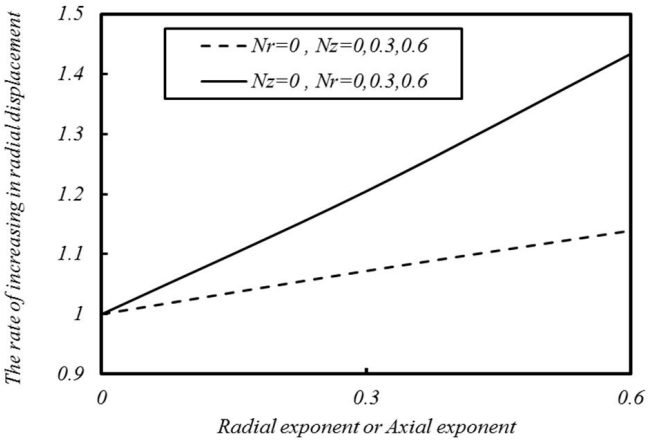

Fig. 6. The rate of increasing in maximum radial displacement for different values of exponent than homogenous porous material

domain (z = 0.5 m and r = 1.5 m in Figure 4) for different values N_r and N_z are calculated and shown in Table 2. It is concluded when the radial exponent is increased, the maximum values of radial stress are increased up to 12%. The variation in the value of axial exponent (N_z) has a negligible effect on the dynamic behavior of radial stress.

Table 2. The maximum of radial stress at the center of domain (z = 0.5 m and r = 1.5 m in Figure 4) in various factor of fgm

σ_{rr}(m)		N_r		
		0	**0.3**	**0.6**
N_z	0	4.33e+5	4.61e+5	4.88e+5
	0.3	4.34e+5	4.62e+5	4.89e+5
	0.6	4.35e+5	4.63e+5	4.89e+5

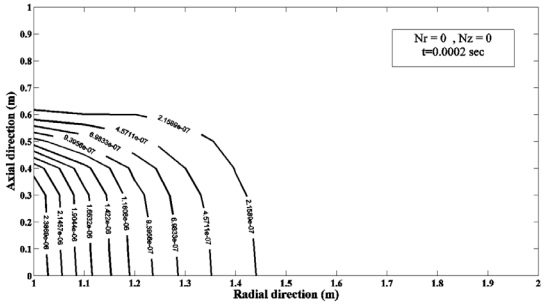

A) t = 0.0002 sec

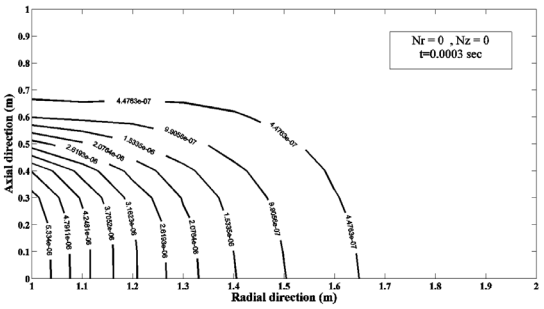

A) t = 0.0003 sec

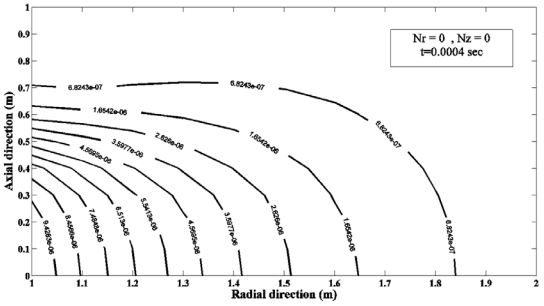

A) t = 0.0004 sec

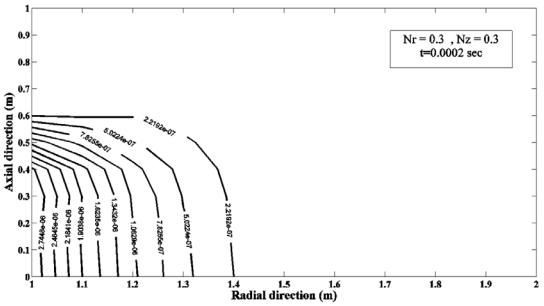

B) t = 0.0002 sec

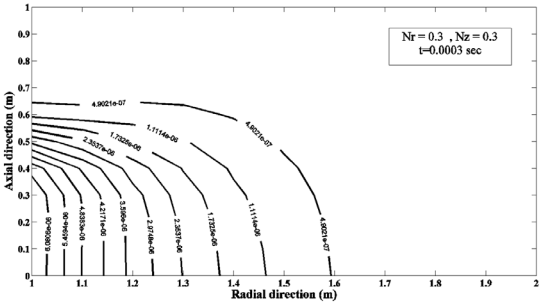

B) t = 0.0003 sec

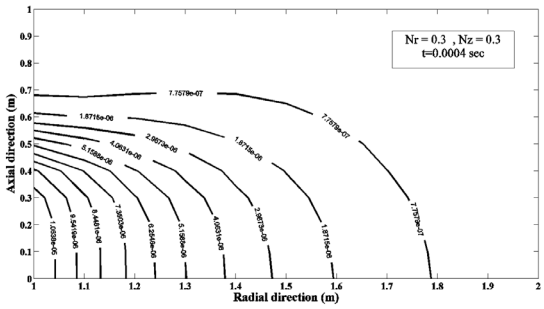

B) t = 0.0004 sec

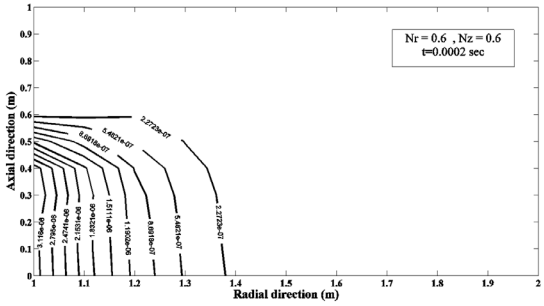

C) t = 0.0002 sec

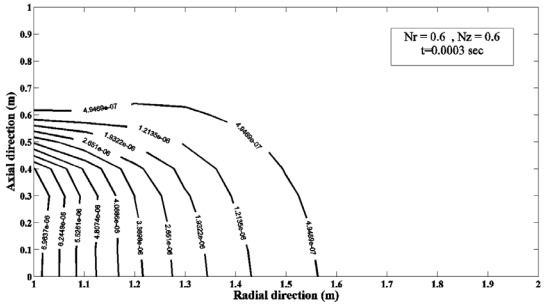

C) t = 0.0003 sec

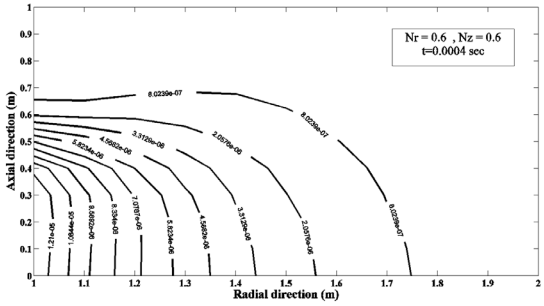

C) t = 0.0004 sec

Fig. 7. The radial displacement time histories at node 1 for various 2D-FGM two dimensional radial displacement wave propagation for A) $N_r = 0$, $N_z = 0$, B) $N_r = 0.3$, $N_z = 0.3$, C) $N_r = 0.6$, $N_z = 0.6$ at various times

The values of radial displacement of two different nodes in various factors of FGM at two times are calculated in Table 3. Accordingly, when the radial and axial exponents are increased, the percentage of difference of radial displacement between the two points is increased. It should be noted that the difference in displacement will decrease, as time passes and the wave front reaches all the points of the domain.

Table 3. The percentage of difference of radial displacement at two points in various factors of fgm in two different time

u_r (m)	$N_z = N_r$	$z = 0.5$ $r = 1$	$z = 0.5$ $r = 1.5$	The percentage of difference of radial displacement
t=0.0003	0	2.85e-6	5.13e-7	82
	0.3	3.40e-6	4.18e-7	87
	0.6	3.93e-6	3.25e-7	92
t=0.0005	0	7.67e-6	2.85e-6	62
	0.3	9.22e-6	2.88e-6	68
	0.6	1.08e-5	2.90e-6	73

Figure 8 depicts the distributions of radial stress in the homogenous porous material along r direction at the various time instants for $z = 0$. It is evident that the stress wave propagates with finite speed through r direction. The velocity of stress wave propagation is dependent on the assumed mechanical properties of the porous field. In this figure, the radial stress wave front can be tracked at various time instants. Also, the wave fronts of radial stress can be observed in three dimensional graphs for homogenous porous material at different time instants in Figure 9.

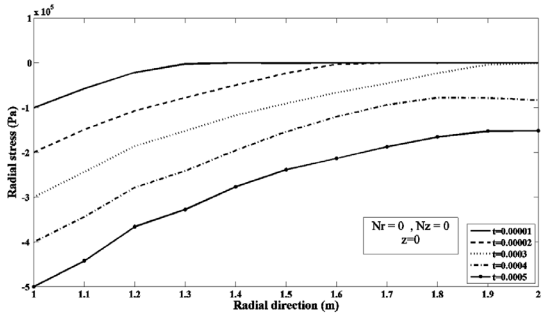

Fig. 8. The distributions of radial stress along radial direction at the various time instants

6- Conclusions

A meshless technique based on the MLPG method with heaviside step function as the weight function is employed to investigate the effects of the material gradation on displacements and stresses wave propagation in the porous medium around the borehole, which is subjected to the shock loading. For this purpose, two dimensional exponential grading patterns for the shear modulus, coupling parameters between the solid and fluid and permeability are considered in the excavation disturbed zone. To interpolate the fields' variables in terms of its nodal values, the radial point interpolation method (RPIM) with radial basis function (RBF) is used. The main results of the presented research can be summarized as follows:

- The MLPG method shows that it is a very effective method with a high accuracy for stress and displacement

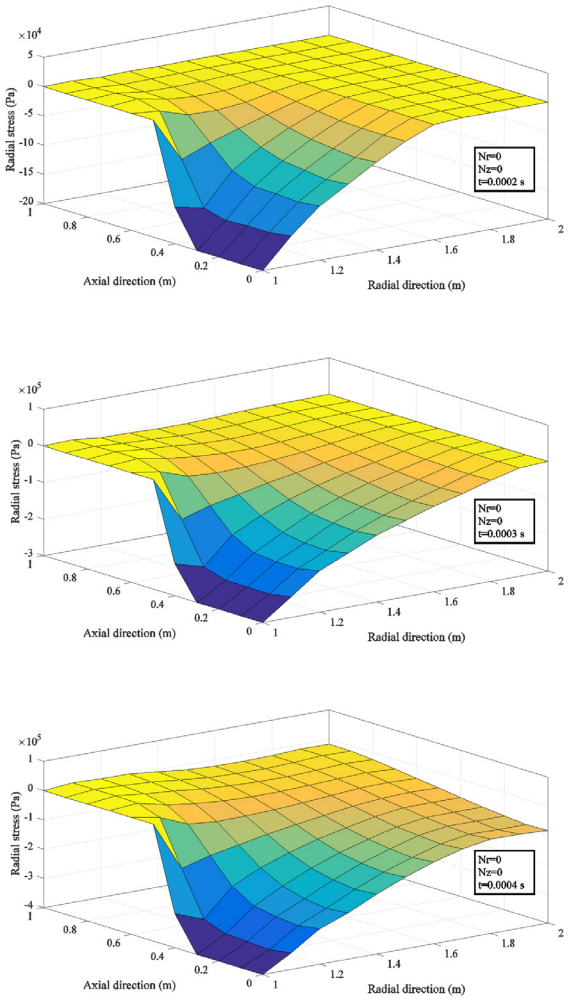

Fig. 9. Two dimensional radial stress wave propagation for N_r=0, N_z=0 at various times A) t = 0.0002 sec, B) t = 0.0003 sec, C) t = 0.0004 sec

propagation analysis of saturated porous materials with one and two directional grading patterns.

- The effects of various grading patterns on the dynamic behaviors of displacements and stresses are obtained and discussed in detail.
- The variation in the value of radial exponent (N_r) has more effect on the dynamic behavior of radial displacement and radial stress compared to the variation in the value of axial exponent (N_z).
- By increasing the value of the exponent, the wave propagation speed is decreased but the values of radial displacement contours are increased.
- The stresses and displacements wave fronts are tracked in two dimensional domains for various grading patterns at different periods of time.

References

[1] K. Terzaghi, *Erdbaumechanik auf bodenphysikalischer Grundlage*, (1925).

[2] M.A. Biot, General theory of three-dimensional consolidation, *Journal of applied physics*, 12(2) (1941) 155-164.

[3] A.P. Selvadurai, *Mechanics of poroelastic media*, Springer Science & Business Media, 2013.

[4] M. Schanz, Poroelastodynamics: linear models, analytical solutions, and numerical methods, *Applied mechanics reviews*, 62(3) (2009) 030803.

[5] M. Schanz, A.-D. Cheng, Transient wave propagation in a one-dimensional poroelastic column, *Acta Mechanica*, 145(1-4) (2000) 1-18.

[6] M.H.G. Rad, F. Shahabian, S.M. Hosseini, A meshless local Petrov–Galerkin method for nonlinear dynamic analyses of hyper-elastic FG thick hollow cylinder with Rayleigh damping, *Acta Mechanica*, 226(5) (2015) 1497-1513.

[7] X. Lai, M. Cai, F. Ren, M. Xie, T. Esaki, Assessment of rock mass characteristics and the excavation disturbed zone in the Lingxin Coal Mine beneath the Xitian river, China, *International Journal of Rock Mechanics and Mining Sciences*, 43(4) (2006) 572-581.

[8] S. Kwon, C. Lee, S. Cho, S. Jeon, W. Cho, An investigation of the excavation damaged zone at the KAERI underground research tunnel, *Tunnelling and underground space technology*, 24(1) (2009) 1-13.

[9] W. Kaewjuea, *Poroelastic solutions for borehole and cylinder*, Chulalongkorn University, 2010.

[10] J. Sladek, V. Sladek, C. Zhang, M. Schanz, Meshless local Petrov-Galerkin method for continuously nonhomogeneous linear viscoelastic solids, *Computational Mechanics*, 37(3) (2006) 279-289.

[11] S. Moussavinezhad, F. Shahabian, S.M. Hosseini, Two-dimensional stress-wave propagation in finite-length FG cylinders with two-directional nonlinear grading patterns using the MLPG method, *Journal of Engineering Mechanics*, 140(3) (2013) 575-592.

[12] S. Chen, C. Xu, G. Tong, A meshless local natural neighbour interpolation method to modeling of functionally graded viscoelastic materials, *Engineering Analysis with Boundary Elements*, 52 (2015) 92-98.

[13] J. Sladek, V. Sladek, M. Schanz, A meshless method for axisymmetric problems in continuously nonhomogeneous saturated porous media, *Computers and Geotechnics*, 62 (2014) 100-109.

[14] J. Sladek, V. Sladek, M. Schanz, The MLPG applied to porous materials with variable stiffness and permeability, *Meccanica*, 49(10) (2014) 2359-2373.

[15] S.M. Hosseini, F. Shahabian, Stochastic assessment of thermo-elastic wave propagation in functionally graded materials (FGMs) with Gaussian uncertainty in constitutive mechanical properties, *Journal of Thermal Stresses*, 34(10) (2011) 1071-1099.

[16] S.M. Hosseini, F. Shahabian, Transient analysis of thermo-elastic waves in thick hollow cylinders using a stochastic hybrid numerical method, considering Gaussian mechanical properties, *Applied Mathematical Modelling*, 35(10) (2011) 4697-4714.

[17] F. Shahabian, S.M. Hosseini, Stochastic dynamic analysis of a functionally graded thick hollow cylinder with uncertain material properties subjected to shock loading, *Materials & Design*, 31(2) (2010) 894-901.

[18] S.M. Hosseini, F. Shahabian, Reliability of stress field

in Al–Al2O3 functionally graded thick hollow cylinder subjected to sudden unloading, considering uncertain mechanical properties, *Materials & Design*, 31(8) (2010) 3748-3760.

[19] O. Coussy, *Poromechanics*, John Wiley & Sons, 2004.

[20] G. Liu, *1013 Mesh Free Methods: Moving beyond the Finite Element Method*, CRC Press, 2003(16) (2003) 937-938.

[21] E. Detournay, A. Cheng, *Fundamentals of Poroelasticity, volume 2 of Comprehensive Rock Engineering: Principles*, Practice & Projects. Pergamon Press, (1993).

Please cite this article using:

H. Kazemi, F. Shahabian , S. M. Hosseini, Two Dimensional Stress and Displacement Wave Propagation Under Shock Loading in Saturated Porous Materials with Two Dimensional Functionally Graded Materails Using MLPG Method, *AUT J. Civil Eng.*, 1(2) (2017) 167-176.

DOI: 10.22060/ceej.2017.12762.5262